

1 **Threshold Atmospheric Electric Fields for Initiating Relativistic Runaway Electron
2 Avalanches: Theoretical Estimates and CORSIKA Simulations**

4 Ashot Chilingarian*, Liza Hovhannisyan, Mary Zazyan

5 A. I. Alikhanyan National Laboratory (YerPhI), Alikhanyan Brothers 2, Yerevan 0036, Armenia

6 *Corresponding author: chili@aragats.am

7 **Abstract**

10 We examine the threshold atmospheric electric field (E_{th}) required to initiate a runaway
11 avalanche in Earth's atmosphere. We compare the traditional, thirty-year-old theoretical
12 threshold value with its recently updated value, along with the threshold derived from
13 CORSIKA-simulated avalanches (E_z). The altitude dependence of these thresholds is analyzed,
14 considering changes in air density and their effects on avalanche development. This study is
15 vital for understanding high-energy atmospheric phenomena in both the lower and upper
16 atmosphere, including thunderstorm ground enhancements (TGEs) and gamma glows, and for
17 refining atmospheric electric field (AEF) models based on particle flux measurements.

19 **Short Summary**

20 Thunderstorms can accelerate particles in the atmosphere, producing bursts of radiation at
21 the ground. We investigated how strong the electric field inside a cloud must be to initiate
22 such events. Using advanced computer simulations and comparing with measurements
23 from mountain stations, we found that the fields must be stronger than earlier theory
24 suggested. Our results improve understanding of storm electricity and its role in natural
25 radiation.

27 **Highlights**

- 28 • Introduces a refined framework for determining the threshold atmospheric electric fields
29 (E_{th}) required to initiate relativistic runaway electron avalanches (RREAs) and
30 thunderstorm ground enhancements (TGEs).
- 31 • Compares classical ($E_{th} \approx 2.80 \text{ kV/cm} \times n$) and updated ($E_{th} \approx 2.67 \text{ kV/cm} \times n$) theoretical
32 thresholds with altitude-dependent thresholds derived from CORSIKA simulations.
- 33 • Demonstrates that realistic avalanche development requires fields 15–22%
34 stronger than theoretical values, depending on altitude and air density.
- 35 • Provides a reproducible simulation methodology for integrating experimental
36 particle-flux measurements into atmospheric electricity models across multiple
37 research stations.

39 **Introduction**

41 Free electrons are abundant in the troposphere. The altitude at which their **flux** reaches
42 its highest point, called the Regener–Pfotzer maximum (Regener, 1933). It depends on
43 the geomagnetic cutoff rigidity (R_c), the type of particles being measured, and
44 the phase and strength of the solar cycle. Recent observations, supported by PARMA4.0

45 calculations (Sato, 2016), show that at middle to low latitudes ($R_c = 3\text{--}8$ GV), the highest
46 flux of charged particles occurs at altitudes around 12–14 km (see Figure 3 in Ambrozova et
47 al., 2023).

48 Atmospheric electric fields (AEFs) generated by thunderstorms transfer energy to free
49 electrons, accelerate them, and, under certain conditions, induce electron-photon avalanches.
50 In 1992, Gurevich, Milikh, and Roussel-Dupré identified the conditions necessary for
51 extensive multiplication of electrons from an energetic seed electron injected into a strong
52 AEF region (Gurevich et al., 1992). This process is known as the Relativistic Runaway
53 Electron Avalanche (RREA; Babich et al., 2001; Alexeenko et al., 2002). A numerical
54 approach for solving the relativistic Boltzmann equation for runaway electron beams
55 (Symbolisty et al., 1998) aids in estimating the threshold AEF (Babich et al., 2001; Dwyer et
56 al., 2003) required to trigger RREA. As demonstrated by GEANT4 and CORSIKA
57 simulations (Chilingarian et al., 2012, 2022), the RREA process is a threshold phenomenon,
58 with avalanches initiating when the atmospheric AEF exceeds a certain threshold that depends
59 on air density. The AEF must also be sufficiently extended to support the growth of
60 avalanches. At standard temperature and pressure in dry air at sea level, $E_{th} \approx 2.80 \text{ kV/cm} \times$
61 n , where air density n is relative to the International Standard Atmosphere (ISA) sea-level
62 value (see the recent update of the threshold energy $E_{th} \approx 2.67 \text{ kV/cm} \times n$ in Dwyer and
63 Rassoul, 2024). This threshold field is slightly higher than the breakeven field, which
64 corresponds to the electron energy at which minimum ionization occurs. If electrons traveled
65 exactly along AEF lines, it would define the threshold for runaway electron propagation and
66 the start of avalanche formation. However, the paths of electrons deviate due to Coulomb
67 scattering with atomic nuclei and Møller scattering with atomic electrons, causing deviations
68 from the near-vertical AEF. Additionally, secondary electrons produced by Møller scattering
69 are not generated along the field line; therefore, AEFs must exceed the theoretical RREA
70 threshold E_{th} by approximately 10–20% for electrons to run away and trigger an avalanche.
71

72 1. CORSIKA simulations of RREAs reaching the high-altitude stations

73 2.

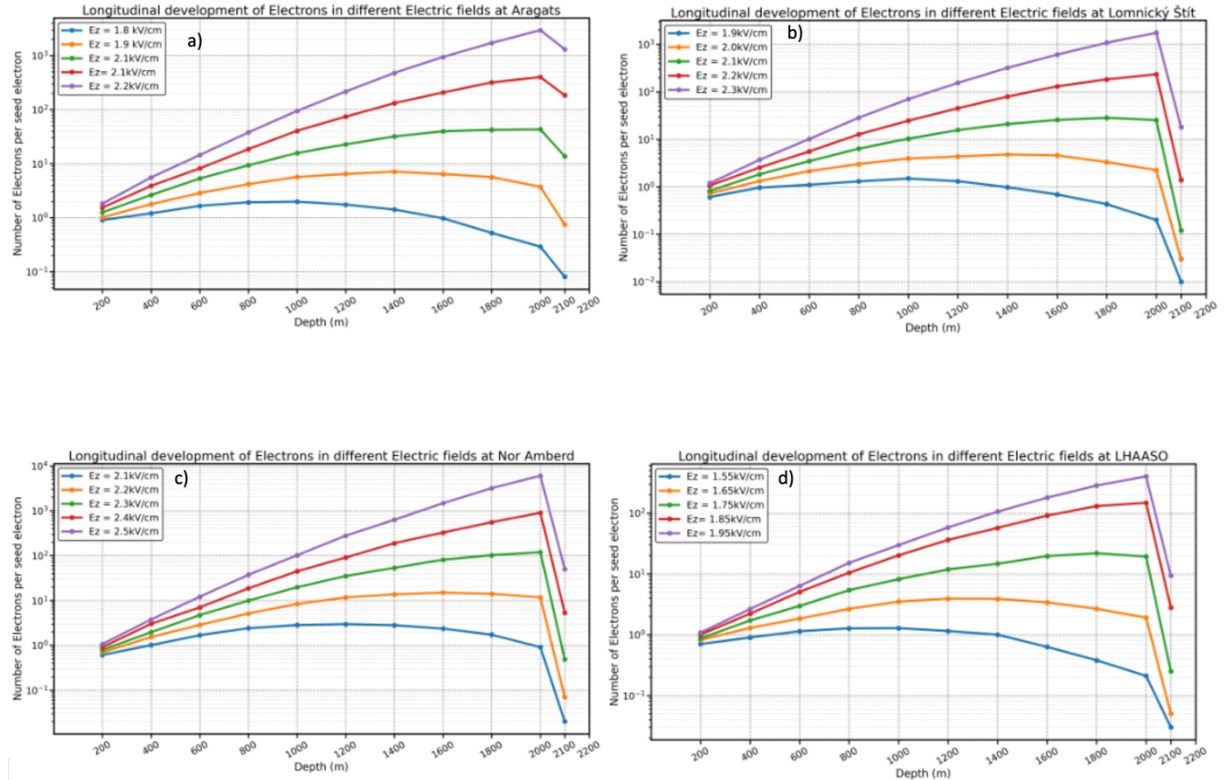
74 To understand how avalanches develop in an electrified atmosphere and to compare the
75 new and updated E_{th} with the particle-intensity abrupt growth, we used the CORSIKA code
76 (Heck et al., 1998), version 7.7500, which accounts for the effect of AEFs on particle
77 transport (Buitink et al., 2009). The growth of RREA increases the cloud's
78 electrical conductivity. Numerous studies (Marshall et al., 1995; Stolzenburg et al., 2007)
79 have indicated that lightning flashes tend to occur when the applied electric field exceeds the
80 RREA threshold by roughly 20–30%.

81 RREA simulation codes do not include a lightning initiation mechanism. Therefore, one
82 can artificially raise the AEF strength beyond a realistic value to produce billions of
83 avalanche particles; however, this approach lacks physical justification. As a result, we
84 do not test AEFs stronger than 2.5 kV/cm at altitudes of 3–6 km. The RREA simulation
85 was performed for vertical seed electrons with a uniform AEF that exceeded the E_{th} by a
86 few tens of percent. An introduced fixed uniform AEF shifts the surplus to E_{th} at different
87 heights by different percentages, corresponding to air density. The chosen seed electron
88 energy spectrum was based on the EXPACS Excel-based program (Sato 2015, Sato 2016),

89 following a power-law with an index of 1.173 for energies from 1 to 300 MeV. During TGE
90 events on Aragats, the typical distance to the cloud base is estimated to be
91 25–200 m (see Figure 17 in Chilingarian et al., 2020); therefore, in our simulations,
92 particle propagation continued in dense air for an additional 25, 50, 100, and
93 200 meters before detection.

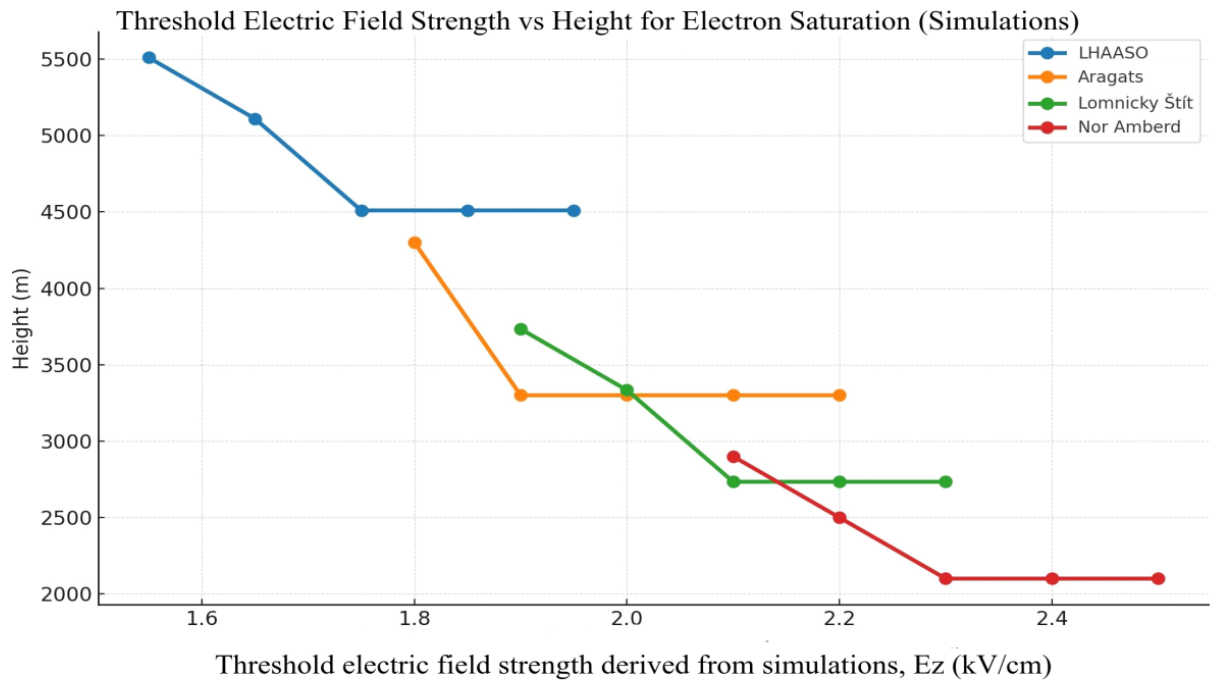
94 The simulations included 1,000 to 10,000 events for AEF strengths from 1.55 to 2.5 kV/cm.
95 Electron and gamma-ray propagation were tracked until their energies dropped to 0.05 MeV.
96 Each simulation event corresponds to the propagation of a single seed electron; **multiple**
97 **events were used to obtain statistically stable averages to reliably estimate**
98 **the resulting threshold electric fields. The CORSIKA code**
99 models the development of RREA by calculating the number of electrons and gamma
100 rays at different stages of the cascade development at 200-meter intervals. At all stations, the
101 atmospheric electric field was implemented as a vertically uniform layer with a thickness of
102 2000 m above the observation levels.

103 Besides the Aragats and Nor Amberd research stations on the slopes of Mt. Aragats in
104 Armenia, we also conducted simulations for the Slovakian and Chinese research stations at
105 Lomnický Štit (Chum et al., 2020) and the Tibetan plateau. LHAASO (Large High Altitude
106 Air Shower Observatory, Aharonian et al., 2023) is situated at 4410 meters above sea level. It
107 provides an ideal platform for studying atmospheric particle acceleration, owing to its thin
108 atmosphere and the high likelihood of runaway electron avalanche formation. For LHAASO,
109 we present CORSIKA simulation results showing increases in electron and photon fluxes
110 under AEF strengths ranging from 1.55 to 1.9 kV/cm. The number of electrons and photons
111 was recorded at **altitudes** ranging from 6510 meters to 4510 meters. Lomnický Štit is located
112 at an altitude of 2630 meters in Slovakia. CORSIKA simulations were performed for various
113 vertical AEFs ranging from 1.9 to 2.3 kV/cm. The number of electrons and photons was
114 recorded at **altitudes** ranging from 4734 meters to 2734 meters. Significant increases in flux
115 were observed with stronger-than-threshold fields, confirming the development of robust
116 RREA. Saturation trends in the growth of electrons and photons suggest that the threshold
117 field, Eth, at Lomnický Štit is approximately 2.3 kV/cm. These results support earlier findings
118 from Aragats and Nor Amberd and emphasize the altitude dependence of Eth. Due to the
119 thinner air at LHAASO, the TGEs occurred at a much lower value of 1.7 kV/cm. In Figures
120 1a-1d, we display the development of RREA at different atmospheric depths and for various
121 physically justified strengths of the AEF. The curves are scaled for a single seed electron for
122 easier comparison with experimentally measured intensities.
123 **For large values of AEFs, the number of avalanche particles rose exponentially. For lower**
124 **values of AEF, we observe saturation of the particle flux when AEF becomes lower than the**
125 **threshold electric field (dependent on air density); the RREA process attenuates before**
126 **reaching the observation level (see the yellow and blue curves in Figures 1a-d).**



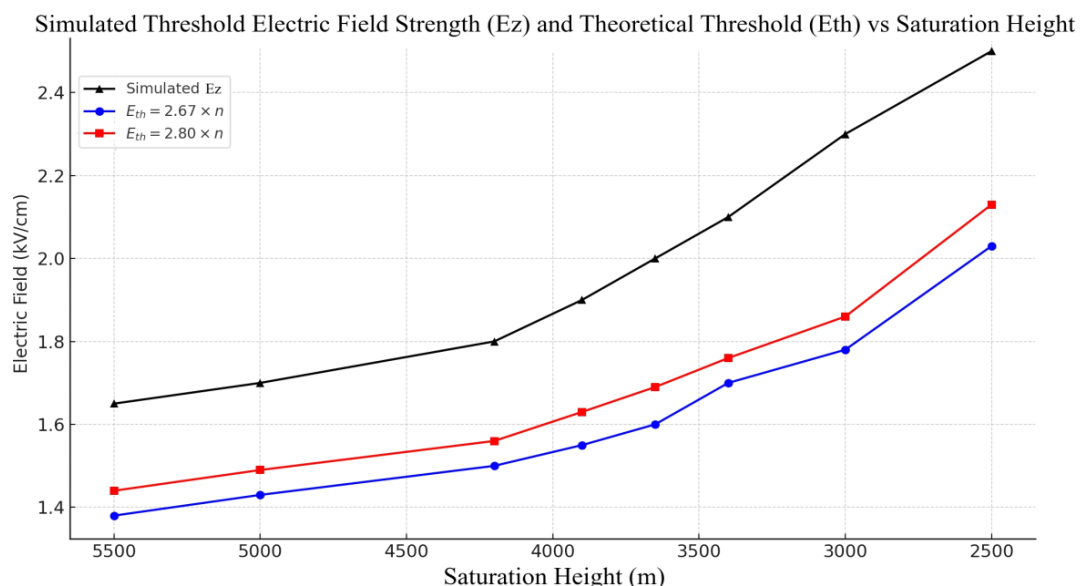
127
128 *Figure 1. Longitudinal development of relativistic runaway electron avalanches (RREA) at*
129 *four high-altitude observation sites: (a) Aragats, (b) Lomnický Štít, (c) Nor Amberd, and (d)*
130 *LHAASO. The number of electrons is normalized to a single seed electron and shown as a*
131 *function of depth within the electric field region. For each site, simulations were performed*
132 *for several electric field strengths, as indicated in the legends. Avalanche development is*
133 *sampled every 200 m across the field region. After exiting the electric field, electron*
134 *propagation is followed for an additional 100 m in free space before reaching the detector.*

135
136 Figure 1 illustrates the dependence of electron multiplication on electric field strength and
137 highlights the altitude-dependent conditions required for sustained avalanche development.
138 We estimate the “simulated” thresholds, E_z values, at the heights where the number of
139 avalanche particles stops rising, as shown in Figure 2.
140



141
142 *Figure 2. Simulated threshold electric field strength, Ez, versus altitude for several high-*
143 *altitudes stations. The threshold is defined as the electric field strength at which the growth of*
144 *avalanche electrons saturates.*

145
146 In Figure 3 and Table 1, we compare the “simulated” threshold Ez with the
147 theoretical ones. Simulations derive higher values than theoretical estimates,
148 especially for high E_{th} values (low altitudes) at all four research stations.
149 Theoretical threshold fields are computed as $2.67 \text{ kV/cm} \times n$ and $2.80 \text{ kV/cm} \times n$.
150 The percentage of enhancement indicates how much the applied field exceeds the
151 theoretical thresholds. Strong AEFs, where the cascade did not attenuate, were not
152 included in the table.



154 *Figure 3. Simulated threshold electric field strength, E_z , and theoretical threshold electric*
 155 *fields, E_{th} , as a function of saturation (rise stopping) altitude.*

156
 157 *Table 1. Excess of E_z over E_{th} . Stopping altitudes and theoretical threshold field comparisons for*
 158 *heights 2500- 5550 m.*

Input E_z (kV/cm)	Enhancement Stopsath(m)	n (relative density)	2.67×n (kV/cm)	2.80×n (kV/cm)	Rel. Excess. (%) (2.80 kV/cm)	Rel. Excess. (%) (2.67 kV/cm)	Station
1.55	5510	0.465	1.24	1.30	19.0	24.8	LHAASO (4400m)
1.65	5110	0.492	1.31	1.38	19.8	25.7	LHAASO (4400m)
1.8	4200.0	0.558	1.49	1.56	15.2	20.8	Aragats (3200m)
1.9	3900.0	0.582	1.55	1.63	16.6	22.3	Aragats (3200m)
1.9	3734	0.595	1.59	1.67	14.0	19.5	Lomnický Štít(2630 m)
2.0	3334	0.629	1.68	1.76	13.5	19.0	Lomnický Štít(2630 m)
2.1	2700.0	0.687	1.84	1.92	9.1	14.4	Nor Amberd (2000m)
2.2	2500.0	0.707	1.89	1.98	11.2	16.6	Nor Amberd (2000m)

159
 160 **2. Discussion and conclusion**
 161
 162 Both the classical threshold field ($E_{th} \approx 2.80 \text{ kV/cm} \times n$) and its updated
 163 version ($E_{th} \approx 2.67 \text{ kV/cm} \times n$) are derived under idealized assumptions; the difference
 164 between them results from refinements in modeling particle energy loss processes. The
 165 earlier estimate of $2.80 \text{ kV/cm} \times n$ was based on basic energy balance considerations using
 166 older ionization loss models and assumed monoenergetic electrons. This threshold
 167 is slightly above the breakeven field, where energy gain equals average energy loss.
 168 The updated $2.67 \text{ kV/cm} \times n$ value, introduced by Dwyer and Rassoul (2024),
 169 incorporates more accurate relativistic Boltzmann solutions, improved ionization
 170 and bremsstrahlung cross-sections, and a probabilistic treatment of runaway thresholds
 171 across realistic energy spectra. While both thresholds assume idealized, field-aligned
 172 electron motion in a uniform medium, the updated value is physically more consistent.
 173 It predicts a slightly lower field strength needed for initial runaway.

174 However, CORSIKA simulations show that this refined threshold is insufficient for sustained
175 avalanche growth under real atmospheric conditions due to scattering and finite path
176 effects. Moreover, it deviates more from the simulated value than the “classical”,
177 30-year-old estimate. Multiple physical processes inhibit ideal runaway propagation.
178 Coulomb scattering with atmospheric nuclei and Møller scattering with electrons
179 cause substantial angular deflection and energy redistribution. Secondary electrons are
180 not generated strictly along the field direction, and many lose energy before gaining
181 sufficient momentum to continue avalanche growth. As a result, electrons must be
182 accelerated in fields stronger than the threshold to overcome these losses and maintain
183 avalanche conditions. CORSIKA simulations, which incorporate all major interaction
184 mechanisms—including Coulomb and Møller scattering, bremsstrahlung losses, finite
185 propagation distances, and realistic secondary cosmic ray spectra—show that avalanches fully
186 develop only when the applied field exceeds the theoretical threshold by a measurable margin.
187 For the updated $2.67 \text{ kV/cm} \times n$ value, we observe a required excess of approximately 20–22%
188 at the Aragats station (~ 3200 – 4200 m a.s.l.), whereas for the classical $2.80 \text{ kV/cm} \times n$
189 threshold, the excess is typically 15–17%. Interestingly, this required excess decreases with
190 increasing air density, as observed in the Nor Amberd simulations. At lower altitudes (~ 2500 –
191 2700 m a.s.l.), the difference between the applied and threshold fields is reduced: only 14–16%
192 above $2.67 \text{ kV/cm} \times n$, and about 9–11% above $2.80 \text{ kV/cm} \times n$.

193 This trend can be explained as follows:

194 In denser air, the chances of energy-loss interactions increase, but so does the likelihood
195 of electron multiplication through ionization and bremsstrahlung over shorter distances.
196 The avalanche can develop more quickly because seed electrons encounter more target
197 atoms in a given path length. As a result, the necessary “headroom” above the threshold
198 field for sustained multiplication is smaller. Simply put, the efficiency of avalanche
199 formation improves in denser air, even though the absolute threshold field is higher. This
200 results in a smaller relative excess being required above the theoretical threshold.
201 Therefore, although the threshold field scales linearly with air density, the required
202 enhancement factor does not. It decreases with increasing density due to a balance
203 between energy loss and multiplication processes, all of which are faithfully captured in
204 the CORSIKA simulation framework. This emphasizes the importance of altitude-dependent
205 analysis in interpreting Thunderstorm Ground Enhancements (TGEs) and
206 suggests that scaling laws based solely on density may overlook subtler effects arising
207 from atmospheric structure and shower development dynamics. **Among these effects is the local**
208 **temperature profile, which can modify air density and, consequently, slightly affect the effective**
209 **threshold field. A more detailed treatment incorporating measured or modeled temperature**
210 **profiles could further refine threshold estimates for individual events; however, such event-**
211 **specific modeling is beyond the scope of the present work.**

212

213 **3. Code and data availability**

214

215 All materials under the authors’ control that are required to reproduce the results presented
216 in this manuscript are publicly available in a Zenodo repository:

217 <https://doi.org/10.5281/zenodo.17986152>

218

219 The Zenodo archive is organized as follows:

220

221 [code/](#)

222 This directory contains auxiliary materials and user-level post-processing codes
223 (e.g., easread.f) required to ensure the reproducibility of the simulations. These codes
224 were used to analyze the output data of the CORSIKA simulations and to derive the
225 numerical results presented in the manuscript.

226

227 **inputs/**

228 This directory contains all CORSIKA input files used in the simulations for each observation
229 site, including the complete input cards and definitions of the thunderstorm electric-field
230 configurations (el.input, elfield.c), observation levels, energy cutoffs, and all relevant
231 simulation parameters.

232

233 **data/**

234 This directory contains the CORSIKA simulation output files (DAT files) corresponding to
235 the electric-field configurations and observation sites analyzed in the manuscript. The data
236 are organized by station and electric-field strength.

237

238 **tables/**

239 This directory contains the final numerical tables used in the manuscript, including threshold
240 electric-field values, stopping altitudes, relative air densities, and percentage excesses over
241 theoretical thresholds.

242

243 **figures/**

244 This directory contains all figures included in the manuscript, generated directly from the
245 simulation output and the processed numerical data.

246

247 In addition, the repository root contains the official technical documentation of the CORSIKA
248 simulation framework (CORSIKA_GUIDE7.7550.pdf) and a README file describing the
249 structure and contents of the archive.

250

251 The CORSIKA simulation framework is a licensed third-party Monte Carlo code developed
252 and maintained by the Karlsruhe Institute of Technology (KIT). The exact CORSIKA version
253 used in this work is specified in the manuscript and is available for scientific use directly
254 from the official KIT distribution portal. All user-provided inputs, configurations, auxiliary
255 codes, and simulation outputs required for reproducibility are provided in the Zenodo archive.

256

257 Together, these materials ensure full reproducibility of the simulations and results presented in
258 this study for any user with legitimate access to the CORSIKA framework.

259

260 **Author contribution**

261 AC and MZ designed the simulation experiments with the CORSIKA code, and LH
262 performed the simulations. AC prepared the manuscript with contributions from all co-
263 authors

264

265 **Acknowledgment**

266 The authors acknowledge the support of the Science Committee of the Republic of Armenia
267 (Research Project No. 21AG~1C012)
268
269

270 **References**

271 **Aharonian, F., An, Q., Axikegu, et al. (2023).**

272 Flux variations of cosmic ray air showers detected by LHAASO-KM2A during a
273 thunderstorm on 10 June 2021. *Chin. Phys. C* **47**. 015001.

274 <https://doi.org/10.1088/1674-1137/ac3f5b>

275

276 **Alexeenko, V. V., Khaerdinov, N. S., Lidvansky, A. S., et al. (2002).**

277 Transient variations of secondary cosmic rays due to atmospheric electric field and evidence
278 for pre-lightning particle acceleration. *Phys. Lett. A*, **301**, 299–306.
279 [https://doi.org/10.1016/S0375-9601\(02\)00981-7](https://doi.org/10.1016/S0375-9601(02)00981-7)

280

281 **Ambrozová, I., Kákona, M., Dvořák, R., et al. (2023).**

282 Latitudinal effect on the position of the Regener–Pfotzer maximum investigated by balloon
283 flight HEMERA 2019 in Sweden and balloon flights FIK in Czechia. *Radiat. Prot. Dosim.*,
284 **199**(15–16), 2041.
285 <https://doi.org/10.1093/rpd/ncac299>

286

287 **Babich, L. P., Donskoy, E. N., Kutsyk, I. M., & Kudryavtsev, A. Y. (2001).**

288 Comparison of relativistic runaway electron avalanche rates obtained from Monte Carlo
289 simulations and kinetic equation solution. *IEEE Trans. Plasma Sci.*, **29**(3), 430–438.
290 <https://doi.org/10.1109/27.928940>

291

292 **Buitink, S., Huege, T., Falcke, H., Heck, D., & Kuijpers, J. (2009).**

293 Monte Carlo simulations of air showers in atmospheric electric fields. *Astropart. Phys.*, **33**, 1–
294 10.
295 <https://doi.org/10.1016/j.astropartphys.2009.10.006>

296

297 **Chilingarian, A., Mailyan, B., & Vanyan, L. (2012).**

298 Recovering the energy spectra of electrons and gamma rays coming from thunderclouds.
299 *Atmos. Res.*, **114–115**, 1–7.
300 <https://doi.org/10.1016/j.atmosres.2012.05.008>

301

302 **Chilingarian, A., Hovsepyan, G., Karapetyan, T., et al. (2022).**

303 Development of relativistic runaway avalanches in the lower atmosphere above mountain
304 altitudes. *EPL*, **139**, 50001.
305 <https://doi.org/10.1209/0295-5075/ac8763>

306

307 **Chilingarian, A., Karapetyan, T., Aslanyan, D., & Sargsyan, B. (2024).**

308 Dataset on extreme thunderstorm ground enhancements registered on Aragats in 2023.
309 *Mendeley Data*, V1.

310 <https://doi.org/10.1016/j.dib.2024.110554>

311 **Chum, R., Langer, J., Bas'e, M., Kolla'rik, I., Strha'rsky', G., Diendorfer, J. R. (2020).**

312 Significant enhancements of secondary cosmic rays and electric field at high mountain peak

313 during thunderstorms. *Earth Planets Space* **72**, 28.

314 <https://doi.org/10.1186/s40623-020-01155-9>.

315

316

317 **Dwyer, J. R. (2003).**

318 A fundamental limit on electric fields in air. *Geophys. Res. Lett.*, **30**, 2055.

319 <https://doi.org/10.1029/2003GL017781>

320

321 **Dwyer, G. R., & Rassoul, H. K. (2024).**

322 High energetic radiation from thunderstorms and lightning. In *Lightning Electromagnetics*

323 (Vol. 1, pp. 365–389). IET.

324 <https://doi.org/10.48550/arXiv.1501.02775>

325

326 **Gurevich, G., Milikh, R., & Roussel-Dupré, R. (1992).**

327 Runaway electron mechanism of air breakdown and preconditioning during a thunderstorm.

328 *Phys. Lett. A*, **165**(5), 463–468.

329 [https://doi.org/10.1016/0375-9601\(92\)90348-P](https://doi.org/10.1016/0375-9601(92)90348-P)

330

331 **Heck, D., Knapp, J., Capdevielle, J. N., Schatz, G., & Thouw, T. (1998).**

332 CORSIKA: A Monte Carlo code to simulate extensive air showers. Report FZKA-6019,

333 Forschungszentrum Karlsruhe.

334 <https://doi.org/10.5445/IR/270043064>

335

336 **Marshall, T. C., McCarthy, M. P., & Rust, W. D. (1995).**

337 Electric field magnitudes and lightning initiation in thunderstorms *J. Geophys. Res.*, **100**,

338 7097–7103. <https://doi.org/10.1029/95JD00020>

339 **Regener E. (1933).**

340 The intensity of penetrating ultra-radiation in the atmosphere.

341 *Zeitschrift für Physik*, **80**, 174–183 (1933)

342 "

343

344

345 **Sato, T. (2016).**
346 Analytical model for estimating the zenith angle dependence of terrestrial cosmic-ray fluxes.
347 *PLoS ONE*, **11**, e0160390.
348 <https://doi.org/10.1371/journal.pone.0160390>
349

350 **Stolzenburg, M., Marshall, T. C., Rust, W. D., Bruning, E., MacGorman, D. R., &**
351 **Hamlin, T. (2007).**
352 Electric field values observed near lightning flash initiations. *Geophys. Res. Lett.*, **34**, L04804.
353 <https://doi.org/10.1029/2006GL028777>
354

355 **Symbalisty, E. M. D., Roussel-Dupré, R. A., & Yukhimuk, V. A. (1998).**
356 Finite volume solution of the relativistic Boltzmann equation for electron avalanche studies.
357 *IEEE Trans. Plasma Sci.*, **26**, 1575–1582.
358 <https://doi.org/10.1109/27.736065>
359
360
361
362